PAPER

Modeling and simulations of a nonlinear granular metamaterial: application to geometric phase-based mass sensing

To cite this article: M Arif Hasan and Pierre A Deymier 2022 *Modelling Simul. Mater. Sci. Eng.* **30** 074002

IOP Publishing Modelling and Simulation in Materials Science and Engineering
Modelling Simul. Mater. Sci. Eng. **30** (2022) 074002 (14pp) https://doi.org/10.1088/1361-651X/ac8c5f

Modeling and simulations of a nonlinear granular metamaterial: application to geometric phase-based mass sensing

M Arif Hasan[1,*] **and Pierre A Deymier**[2]

[1] Department of Mechanical Engineering, Wayne State University, Detroit, MI 48202, United States of America
[2] Department of Materials Science and Engineering, The University of Arizona, Tucson, AZ 85721, United States of America

E-mail: Hasan.Arif@Wayne.Edu

Received 7 June 2022, revised 20 August 2022
Accepted for publication 24 August 2022
Published 8 September 2022

Abstract

Dynamical simulations of an externally harmonically driven model granular metamaterial composed of four linearly and nonlinearly coupled granules show that the nonlinear normal mode can be expressed in a linear normal mode orthonormal basis with time dependent complex coefficients. These coefficients form the components of a state vector that spans a 2^2 dimensional Hilbert space parametrically with time. Local π jumps in the phase of these components occurring periodically are indicative of topological features in the manifold spanned by the geometric phase of the vibrational state of the metamaterial. We demonstrate that these topological features can be exploited to realize high sensitivity mass sensor. The effect of dissipation on sensitivity is also reported. Nonlinear granular metamaterials with very low dissipation could serve as mass sensors with considerable sensitivity to small mass changes via large changes in geometric phase.

Keywords: geometric phase, Hilbert space, nonlinear normal mode, granular metamaterial, phase-based mass sensor

(Some figures may appear in colour only in the online journal)

Introduction

Most mechanical sensors rely on resonant processes whereby some component vibrates at one of its eigen frequencies. This frequency is therefore sensitive to changes in the device

*Author to whom any correspondence should be addressed.

component properties such as for instance its mass [1]. The sensitivity of the mass sensor increases with the decreasing size of the device. The sensitivity of resonant mass sensors also relies on the ability to measure small changes in resonant frequency. Resonant mechanical sensors effectively measure changes in properties at the interface between the device and the medium to be inspected. Phononic crystal (PnC) sensor also use mechanical resonance but have the ability to sense changes in a bulk medium such as a fluid [2]. Here, the medium under inspection is compartmentalized within the PnC affecting globally its resonant properties. Metamaterial-based sensors may exploit local field enhancement associated with evanescent modes and resonant characteristics to achieve high sensitivity [3]. Resonant sensors rely on shifts in resonances commonly varying linearly with the magnitude of the mass or property perturbations.

Topological attributes of waves such as exceptional points (EP) may also be employed for high sensitivity sensing [4]. EP are degeneracies where eigen modes coalesce. Breaking of system's symmetry that leads to the EP as a result of some perturbation leads to the splitting of the coincident resonant frequencies [5]. In contrast to conventional resonant sensors, this splitting may scale super-linearly with the magnitude of the perturbation leading to enhance sensitivity [6].

The geometric phase is another attribute of topological waves that has to date been excluded from sensing approaches. The total phase of a wave is the sum of the dynamical phase and the geometric wave. The former relates to the time it takes a wave to travel at its velocity along some path in the space it propagates. But the geometric wave depends on the degrees of freedom of this wave that form its abstract parameter space (i.e., the 'space of states' or Hilbert space and not the actual space in which the wave propagates). The state of this wave is a vector in the Hilbert space and the geometric phase depends on the direction of the state vector. The geometric phase accumulated along a path in parameter space represents the change in direction (or 'angle') of the vector state in the Hilbert space given by the Berry connection [7]. External drivers can be used to control the path the state vector spans parametrically in the Hilbert space. The variation of the state vector may be depicted as a geometric manifold whose topology may not be conventional such as Moebius manifolds which exhibits features such as twists. Perturbations such as imperfections, structural defects or simply local or global changes in properties of the system/environment leads, due to scattering, to an additional rotation of the state vector which will follow another parametric path and span a different part of the topological manifold of the wave. Regions of the manifold with sharp topological features such as local twists (associated with sharp π changes in geometric phase) will offer high sensitivity to the presence of perturbations. A recent study has demonstrated the application of geometric phase of seismic waves to sensing changes in environments [8].

In this study, we present a modeling and dynamical simulation investigation of a mass sensor that uses the geometric phase of nonlinear normal modes supported by a granular metamaterial system. An acoustic metamaterial based on coupled granular networks has been the subject of numerous research fields. Impulsively excited acoustic metamaterials were theoretically [9–11] and experimentally [12] studied to passively redirect propagating pulses from a directly excited chain to a single chain or a collection of receiving chains, and to determine the nonlinear mechanisms controlling these energy transfers. In the case of granular metamaterials under harmonic excitations, nonlinear acoustic bands, i.e., pass and stop-bands, and propagating breathers similar to linear periodic systems have also been reported [13, 14]. In the current study, we show that by using external driver that can be controlled through a number of parameters such as the frequency, magnitude and distribution of applied forces, we can express the driven vibrational field of a coupled granular metamaterials in a normal mode orthonormal basis with time dependent complex coefficients. These coefficients represent the components

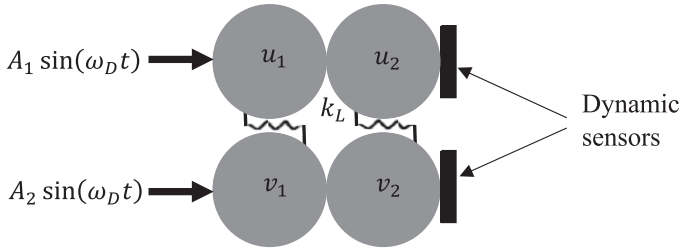

Figure 1. Schematic illustration of the coupled nonlinear granular network. The system is composed of four granules arranged in two granular dumbbell networks. We will refer to the top two granules and bottom two granules as being arranged 'along' the network. The granules within the same dumbbell will be referred as being arranged across the network. External harmonic driving displacements with different amplitudes but same frequency, ω_{D}, are applied on the left granules. The dynamical response of the system is detected on the right. The granules along the network interact via nonlinear Hertzian contact. The granules within a dumbbell interact via linear springs.

of a state vector in the Hilbert space of the granular network. Here, time permits the parametric exploration of paths within this Hilbert space. The time-evolution of the phase associated with these components exhibit sharp feature taking the form of π jumps that can be visualized as twists in the topological manifolds spanned parametrically by time. We show that we can exploit these topological features to create a mass sensor with very high sensitivity. From an experimental point of view, the sensitivity of this phase-based sensor will depend on the ability to accurately measure changes in phase. We also investigate the effect of dissipation on the sensitivity of this metamaterial mass sensor.

1. Non-linear granular metamaterials model system and simulation method

We seek to explore the dynamical response of a metamaterial composed of coupled spherical elastic granules subjected to an external harmonic loading. In a first stage, we consider the granules to be identical. Later, we will address the case of defects in the mass of some of the granules. We assume that all granules are initially in contact with their neighboring granules (cf figure 1). We neglect the effects of gravity; however, the dissipative effect is considered since dissipation is an integral part of any physical system. Due to a small relative displacement of the granules, their rotational degrees of freedom are neglected, which is experimentally feasible by restricting the translational and lateral motions of the granular network.

The general mathematical expression of the equations of motion of the externally driven nonlinear granular network (figure 1), restricted to 1D displacements, reads:

$$\begin{aligned} m\ddot{u}_1 = {} & k_{\mathrm{NL}}[A_1 \sin(\omega_{\mathrm{D}} t) - u_1 + \delta_0]_+^{3/2} \\ & + \eta[A_1\omega \cos(\omega_{\mathrm{D}} t) - \dot{u}_1]H[A_1 \sin(\omega_{\mathrm{D}} t) - u_1 + \delta_0] \\ & - k_{\mathrm{NL}}(u_1 - u_2 + \delta_0)_+^{3/2} - \eta(\dot{u}_1 - \dot{u}_2)H(u_1 - u_2 + \delta_0) + k_{\mathrm{L}}(u_1 - v_1) \\ & + \eta(\dot{u}_1 - \dot{v}_1) \end{aligned}$$

$$\begin{aligned} m\ddot{u}_2 = {} & k_{\mathrm{NL}}(u_1 - u_2 + \delta_0)_+^{3/2} + \eta(\dot{u}_1 - \dot{u}_2)H(u_1 - u_2 + \delta_0) \\ & - k_{\mathrm{NL}}(u_2 + \delta_0)_+^{3/2} - \eta\dot{u}_2 H(u_2 + \delta_0) + k_{\mathrm{L}}(u_2 - v_2) + \eta(\dot{u}_2 - \dot{v}_2) \end{aligned}$$

$$
\begin{aligned}
m\ddot{v}_1 = {} & k_{\mathrm{NL}}[A_1\ \sin(\omega_{\mathrm{D}}t) - v_1 + \delta_0]_+^{3/2} \\
& + \eta[A_1\omega\ \cos(\omega_{\mathrm{D}}t) - \dot{v}_1]H[A_1\ \sin(\omega_{\mathrm{D}}t) - v_1 + \delta_0] \\
& - k_{\mathrm{NL}}(v_1 - v_2 + \delta_0)_+^{3/2} - \eta(\dot{v}_1 - \dot{v}_2)H(v_1 - v_2 + \delta_0) + k_{\mathrm{L}}(v_1 - u_1) \\
& + \eta(\dot{v}_1 - \dot{u}_1) \\
m\ddot{v}_2 = {} & k_{\mathrm{NL}}(v_1 - v_2 + \delta_0)_+^{3/2} + \eta(\dot{v}_1 - \dot{v}_2)H(v_1 - v_2 + \delta_0) - k_{\mathrm{NL}}(v_2 + \delta_0)_+^{3/2} \\
& - \eta\dot{v}_2H(v_2 + \delta_0) + k_{\mathrm{L}}(v_2 - u_2) + \eta(\dot{v}_2 - \dot{u}_2). \qquad (1)
\end{aligned}
$$

In equation (1), $(\alpha)_+ = \alpha$ for $\alpha \geqslant 0$, $(\alpha)_+ = 0$ for $\alpha < 0$ and $H(\cdot)$ is the Heaviside function. u_1 and u_2 are the displacements of mass 1 and 2 in the top two granules, respectively; and v_1 and v_2 are the displacements of the bottom two granules 1 and 2. m is the mass of the granules, the terms with dissipation coefficient, η, model the dissipative effects, and A_1 and A_2 represent the amplitudes of the applied input displacements, respectively. $\delta_0 = \left(\frac{F_0}{A_0}\right)^{3/2}$ is the initial static pre-compression value, where F_0 is the homogeneous static compression force, and the parameter A_0 contains the geometry and material property of the granules and has the form $A_0 = \frac{2E\sqrt{R}}{3\sqrt{2}(1-\nu^2)}$ [15]. k_{L} and k_{NL} represent the linear and nonlinear spring coefficients, respectively. Since the strongly nonlinear coupling, k_{NL}, is owing to Hertzian interactions between granules in compression and to keep the dynamics of model (1) in the strongly nonlinear regime, we have used $k_{\mathrm{NL}} = 1$ and $k_{\mathrm{L}} = 0.01$ for the current study.

If the linear coefficient and the static pre-compression are zero, i.e., $k_{\mathrm{L}} = \delta_0 = 0$, the system becomes a strongly (essentially) nonlinear system with no linear term. Such a system has been studied extensively by several researchers [15–17]. In particular, references [18–20] demonstrated that such nonlinear systems possess standing modes, referred to as nonlinear normal modes (NNMs). NNMs differ from linear normal modes (LNMs) since the granule oscillations in NNMS are not always synchronous, even though their frequencies are the same. Note that in these previous studies, the systems were conservative. In practice, dissipation needs to be considered. Hence, with the presence of damping, we seek the nonlinear normal modes of the coupled network and excite the coupled network with out-of-phase ($A_1 = -A_2$) mode.

We solve the dynamical equation (1) employing molecular dynamics (MD) simulation and have used Runge–Kutta (4) and (5) formula. In the MD simulation, total time-steps of 2^{21} and unit-steps of 0.01 were used to ensure conservation of the total energy with an accuracy better than $1 \times 10^{-11}\%$.

2. Numerical results on the nonlinear dynamics of the granular system

2.1. Nonlinear normal modes

In figure 2 we report the displacement of the four granules as a function of time when we excite the first masses on the left of the network with the out-of-phase mode, i.e., $A_1 = -A_2$ (see figure caption for complete set of model parameters). The top and bottom two granules vibrate out-of-phase. The two top or bottom two granules vibrate in-phase.

Since the coupling stiffness across the network is linear, the eigenstates across the network can be written as $E_1^{\mathrm{Ac}} = \frac{1}{\sqrt{2}}\begin{pmatrix}1\\1\end{pmatrix}$ and $E_2^{\mathrm{Ac}} = \frac{1}{\sqrt{2}}\begin{pmatrix}1\\-1\end{pmatrix}$, where the superscript Ac stands for eigenstates *across* the network. These orthogonal states are mutually exclusive.

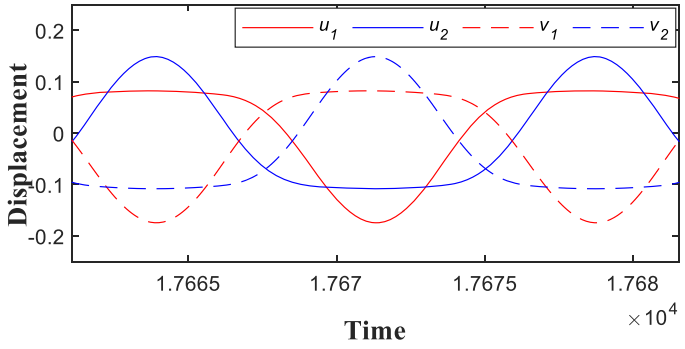

Figure 2. Time series of the granule displacements of the NNM for the coupled granular network. System parameters: $A_1 = \frac{1}{30}, \eta = \frac{2}{900}, \delta_0 = 0, \omega_D = 0.4241, A_2 = -A_1,\ k_{NL} = 1,\ k_L = 0.01$.

We would like to point out that several previous works on wave propagation in bi-modular media, such as backward propagation [21], veering [22], and appearing crossing points between different modes [23], have been published. However, those works could be resolved using analytical approaches based on either continuous approximations or homogenization. On the contrary, from figure 2, we observe that the current granular media dynamics are not only strongly nonlinear (not even linearizable) but also involve both compression and separation between adjacent granules. Hence, the dynamics must consider the non-smooth effects due to the granule separation. The oscillation's non-smooth effects are linked to granule responses' silence intervals, i.e., to motion-phases in which a granule is stationary at a distance from the equilibrium zero. As a result, the normal mode depicted in figure 2 is the mode that is most influenced and driven by the granular system's discrete nature. We will demonstrate how the nonconservative discrete granular metamaterials dynamics' discontinuous character gives rise to intriguing features that will be used in conjunction with the nonseparable states and topology to achieve a high sensitivity mass sensor. The concept of nonseparable states and topology has implications in several branches of physics and has found applications in sensing, in particular quantum sensing [24–27].

The displacement field in figure 2 is the Fourier sum of the linear and nonlinear modes, each with its characteristic frequency. This is revealed in figure 3 through the temporal Fourier transform of the first top granule's displacement. To identify the dominant characteristic frequencies in the coupled network, we set a threshold of 1% of the maximum amplitude to eliminate noise (dotted line in figure 3(a)). Moreover, we calculate the phase differences between granules along and across the network for each dominant characteristic frequency. For example, in figure 3(b), we see that for the lowest dominant characteristic frequency of $\omega = \omega_D = 0.4241$, corresponding to the driving frequency, the phase differences between granules are $\varphi_{u_1,u_2} = \varphi_{u_1} - \varphi_{u_2} = \varphi_{v_1} - \varphi_{v_2} = \varphi_{v_1,v_2} = 0$ and $\varphi_{u_1,v_1} = \varphi_{u_1} - \varphi_{v_1} = \varphi_{u_2} - \varphi_{v_2} = \varphi_{u_2,v_2} = \pi$, where $\varphi_{u_1}, \varphi_{u_2}, \varphi_{v_1}$, and φ_{v_2} are the absolute phases of the granule displacements u_1, u_2, v_1, and v_2. This implies that the displacement field of the granules' network can be described by the eigenstates: $E_1^{Al} = \frac{1}{\sqrt{2}}\begin{pmatrix}1\\1\end{pmatrix}$ and $E_2^{Ac} = \frac{1}{\sqrt{2}}\begin{pmatrix}1\\-1\end{pmatrix}$ at the characteristic frequency ω. The superscript Al stands for eigenstates characterizing modes *along* the network and Ac stands for eigenstates characterizing modes *across* the network. At the second higher harmonics, $2\omega_D$,

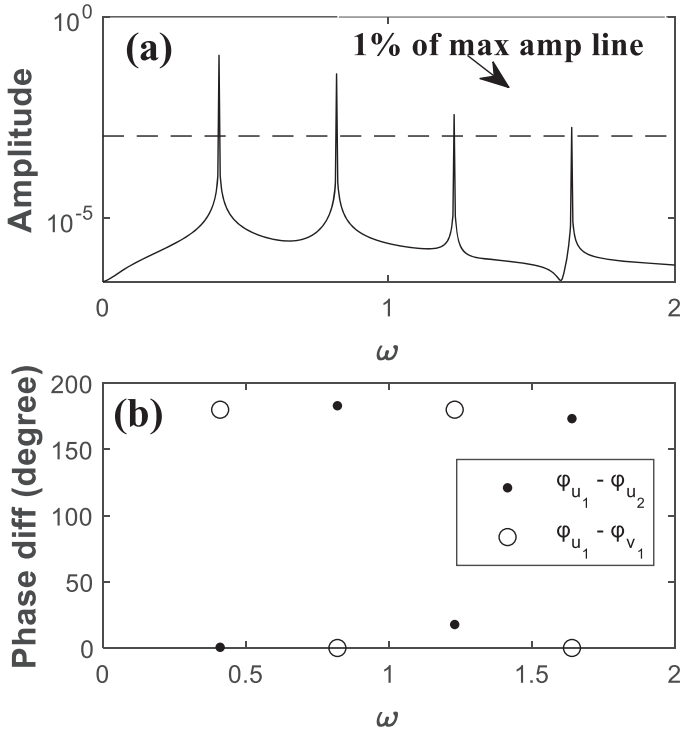

Figure 3. (a) Temporal Fourier transform of the first top granule's displacement, and (b) phase difference between granules at each of the dominant characteristic frequency. In (a), we set a threshold value of 1% of the maximum amplitude (dotted line) to identify the dominant characteristic frequencies.

we observe in figure 3(b) that the phase difference between granules along the network is π while it is 0 across the network. Hence, at this other characteristic frequency, the displacement field can be described by the eigenstates: $E_2^{\mathrm{Al}} = \frac{1}{\sqrt{2}}\begin{pmatrix} 1 \\ -1 \end{pmatrix}$ and $E_1^{\mathrm{Ac}} = \frac{1}{\sqrt{2}}\begin{pmatrix} 1 \\ 1 \end{pmatrix}$.

It is emphasized that even though NNMs do not possess orthogonality properties (as do the linear normal modes) [28–30], the combinations of E_1^{Al} and E_2^{Al}, and E_1^{Ac} and E_2^{Ac} form a complete orthonormal basis for the system. Therefore, we can form a basis for the states of the coupled granular network in the form of four tensor products: $E_1^{\mathrm{Al}} \otimes E_1^{\mathrm{Ac}}$, $E_1^{\mathrm{Al}} \otimes E_2^{\mathrm{Ac}}$, $E_2^{\mathrm{Al}} \otimes E_1^{\mathrm{Ac}}$ and $E_2^{\mathrm{Al}} \otimes E_2^{\mathrm{Ac}}$. In this basis, for any specific characteristic frequency, ω, the displacement field can be written as:

$$\begin{pmatrix} |C_1|\mathrm{e}^{\mathrm{i}\varphi_{u_1}} \\ |C_2|\mathrm{e}^{\mathrm{i}\varphi_{v_1}} \\ |C_3|\mathrm{e}^{\mathrm{i}\varphi_{u_2}} \\ |C_4|\mathrm{e}^{\mathrm{i}\varphi_{v_2}} \end{pmatrix} \mathrm{e}^{\mathrm{i}\omega t} = \big(A_{11}E_1^{\mathrm{Al}} \otimes E_1^{\mathrm{Ac}} + A_{12}E_1^{\mathrm{Al}} \otimes E_2^{\mathrm{Ac}} + A_{21}E_2^{\mathrm{Al}} \otimes E_1^{\mathrm{Ac}} + A_{22}E_2^{\mathrm{Al}} \otimes E_2^{\mathrm{Ac}}\big)\mathrm{e}^{\mathrm{i}\omega t},$$

where $C_i, i = 1, 2, 3, 4$, are the amplitudes at each of the specific characteristic frequency ω. $A_{ij}, i, j = 1, 2$, are the amplitude coefficients associated with each product state. Simplifying the above equation leads to:

$$\begin{pmatrix} |C_1|e^{i\varphi_1} \\ |C_2|e^{i\varphi_2} \\ |C_3|e^{i\varphi_3} \\ |C_4|e^{i\varphi_4} \end{pmatrix} = \frac{1}{2}\begin{pmatrix} A_{11} + A_{12} + A_{21} + A_{22} \\ A_{11} - A_{12} + A_{21} - A_{22} \\ A_{11} + A_{12} - A_{21} - A_{22} \\ A_{11} - A_{12} - A_{21} + A_{22} \end{pmatrix}. \tag{2}$$

Using equation (2), we can calculate each product state's amplitude coefficients, A_{ij}; $i, j = 1, 2$, associated with each dominant characteristic frequency. The amplitudes, A_{ij}, are complex quantities. Hence, similarly to a quantum system, after normalization of equation (2), a unit vector can be used to describe the state of the granular network in a complex vector space (or inner product space), known as state space or Hilbert space. Moreover, the vectors E_1^{Al} and E_2^{Al} are two mutually orthogonal eigenstates along the granular network and therefore, form an orthonormal basis for a two-dimensional Hilbert space, $H_{E^{\mathrm{Al}}}$. Similarly, the vectors E_1^{Ac} and E_2^{Ac} are two mutually orthogonal eigenstates across the network and hence form an orthonormal basis for another two-dimensional Hilbert space, $H_{E^{\mathrm{Ac}}}$. Therefore, using an analogy with a quantum system, we use the Dirac notation for vectors and apply it to the elastic states of the coupled granular network by writing vectors in state space as:

$$\begin{pmatrix} |C_1|e^{i\varphi_1} \\ |C_2|e^{i\varphi_2} \\ |C_3|e^{i\varphi_3} \\ |C_4|e^{i\varphi_4} \end{pmatrix} = \big(A_{11}\big|E_1^{\mathrm{Al}}\big\rangle\big|E_1^{\mathrm{Ac}}\big\rangle + A_{12}\big|E_1^{\mathrm{Al}}\big\rangle\big|E_2^{\mathrm{Ac}}\big\rangle + A_{21}\big|E_2^{\mathrm{Al}}\big\rangle\big|E_1^{\mathrm{Ac}}\big\rangle + A_{22}\big|E_2^{\mathrm{Al}}\big\rangle\big|E_2^{\mathrm{Ac}}\big\rangle\big)e^{i\omega t}. \tag{3}$$

By doing so, we define the orthonormal basis as $|\phi_1\rangle = \big|E_1^{\mathrm{Al}}\big\rangle\big|E_1^{\mathrm{Ac}}\big\rangle, |\phi_2\rangle = \big|E_1^{\mathrm{Al}}\big\rangle\big|E_2^{\mathrm{Ac}}\big\rangle, |\phi_3\rangle = \big|E_2^{\mathrm{Al}}\big\rangle\big|E_1^{\mathrm{Ac}}\big\rangle$ and $|\phi_4\rangle = \big|E_2^{\mathrm{Al}}\big\rangle\big|E_2^{\mathrm{Ac}}\big\rangle$, i.e., as products of eigenstates along and across the granular network. Accordingly, $|\phi_1\rangle, |\phi_2\rangle, |\phi_3\rangle$ and $|\phi_4\rangle$ form the basis of a four-dimensional Hilbert product space $H_{E^{\mathrm{Al}},E^{\mathrm{Ac}}} = H_{E^{\mathrm{Al}}} \otimes |H_{E^{\mathrm{Ac}}}$, where $H_{E^{\mathrm{Al}}}$ is the space associated with the degrees of freedom along the granular network with basis $\left\{E_1^{\mathrm{Al}}, E_2^{\mathrm{Al}}\right\}$, and $H_{E^{\mathrm{Ac}}}$ representing degrees of freedom across the network with basis $\left\{E_1^{\mathrm{Ac}}, E_2^{\mathrm{Ac}}\right\}$. The states of the granular network can be thought of as the states of a two partite composite system with one subsystem associated with the degrees of freedom along the network and the second subsystem associated with the degrees of freedom across the network. Each subsystem is effectively a two-level system. The dimension of the Hilbert space $H_{E^{\mathrm{Al}}}$ is 2. The space $H_{E^{\mathrm{Ac}}}$ is also two-dimensional. The dimension of the product space is therefore four-dimensional $2^2 = 4$.

2.2. Time dependent complex amplitudes and phases of granule displacement

At each of the characteristic frequencies identified in figure 3(a), we write the displacement field by using equation (3). Moreover, through construction, if we write the displacement field as a tensor product of linear combinations of eigenstates, i.e., as a tensor product of the linear

combination of eigenstates along and across the granular network, we obtain:

$$\begin{pmatrix} |C_1|e^{i\varphi_1} \\ |C_2|e^{i\varphi_2} \\ |C_3|e^{i\varphi_3} \\ |C_4|e^{i\varphi_4} \end{pmatrix} = \left[\left(\alpha\left|E_1^{\mathrm{Al}}\right\rangle + \beta\left|E_2^{\mathrm{Al}}\right\rangle\right) \otimes \left(\gamma\left|E_1^{\mathrm{Ac}}\right\rangle + \delta\left|E_2^{\mathrm{Ac}}\right\rangle\right)\right] e^{i\omega t} \tag{4}$$

this is only possible if $\alpha\gamma = A_{11}, \alpha\delta = A_{12}, \beta\gamma = A_{21}, \beta\delta = A_{22}$, where $\alpha, \beta, \gamma, \delta \in \mathbb{R}$. In this case, the state is a separable state. If the displacement field cannot be written as a product of a linear combination of eigenstates along and across the granular network, the state is a non-separable state. In analogy with quantum mechanics, this can be interpreted as classical 'entanglement' since it possesses the quantum mechanical feature of non-factorizability, though it lacks non-locality [31–36].

The coefficients, A_{ij}, take on different values for each of the characteristic frequencies, ω_n. Hence, the total displacement field of the coupled granular network can be written as the linear combination:

$$\begin{aligned} \vec{U} &= \sum_n \begin{pmatrix} |C_{1,n}|e^{i\varphi_{1,n}} \\ |C_{2,n}|e^{i\varphi_{2,n}} \\ |C_{3,n}|e^{i\varphi_{3,n}} \\ |C_{4,n}|e^{i\varphi_{4,n}} \end{pmatrix} e^{i\omega_n t} \\ &= \sum_n \left(A_{11,n}\left|E_1^{\mathrm{Al}}\right\rangle\left|E_1^{\mathrm{Ac}}\right\rangle + A_{12,n}\left|E_1^{\mathrm{Al}}\right\rangle\left|E_2^{\mathrm{Ac}}\right\rangle + A_{21,n}\left|E_2^{\mathrm{Al}}\right\rangle\left|E_1^{\mathrm{Ac}}\right\rangle \right. \\ &\quad \left. + A_{22,n}\left|E_2^{\mathrm{Al}}\right\rangle\left|E_2^{\mathrm{Ac}}\right\rangle\right) e^{i\omega_n t} \\ &= \sum_n \left(A_{11,n}\, e^{i\omega_n t}\right)\left|E_1^{\mathrm{Al}}\right\rangle\left|E_1^{\mathrm{Ac}}\right\rangle + \sum_n \left(A_{12,n}\, e^{i\omega_n t}\right)\left|E_1^{\mathrm{Al}}\right\rangle\left|E_2^{\mathrm{Ac}}\right\rangle \\ &\quad + \sum_n \left(A_{21,n}\, e^{i\omega_n t}\right)\left|E_2^{\mathrm{Al}}\right\rangle\left|E_1^{\mathrm{Ac}}\right\rangle + \sum_n \left(A_{22,n}\, e^{i\omega_n t}\right)\left|E_2^{\mathrm{Al}}\right\rangle\left|E_2^{\mathrm{Ac}}\right\rangle. \end{aligned} \tag{5}$$

The total displacement field is now expanded on the basis of the product Hilbert space $H_{E^{\mathrm{Al}},E^{\mathrm{Ac}}}$ with time dependent complex coefficients.

In that basis, the total displacement field can be written in the form of a column displacement state vector, $|\psi\rangle$:

$$|\psi\rangle = \begin{pmatrix} \psi_{00} \\ \psi_{01} \\ \psi_{10} \\ \psi_{11} \end{pmatrix} = \begin{pmatrix} \sum_n A_{11,n}\, e^{i\omega_n t} \\ \sum_n A_{12,n}\, e^{i\omega_n t} \\ \sum_n A_{21,n}\, e^{i\omega_n t} \\ \sum_n A_{22,n}\, e^{i\omega_n t} \end{pmatrix}, \tag{6}$$

where, $\psi_{ij}, i, j = 0, 1$ are time dependent complex coefficients.

The simplest necessary condition for such a state to being classically entangled (i.e., non-separable into a product) is $\left(\sum_n A_{11,n}\, e^{i\omega_n t}\right)\left(\sum_n A_{22,n}\, e^{i\omega_n t}\right) \neq \left(\sum_n A_{12,n}\, e^{i\omega_n t}\right)\left(\sum_n A_{21,n}\, e^{i\omega_n t}\right)$.

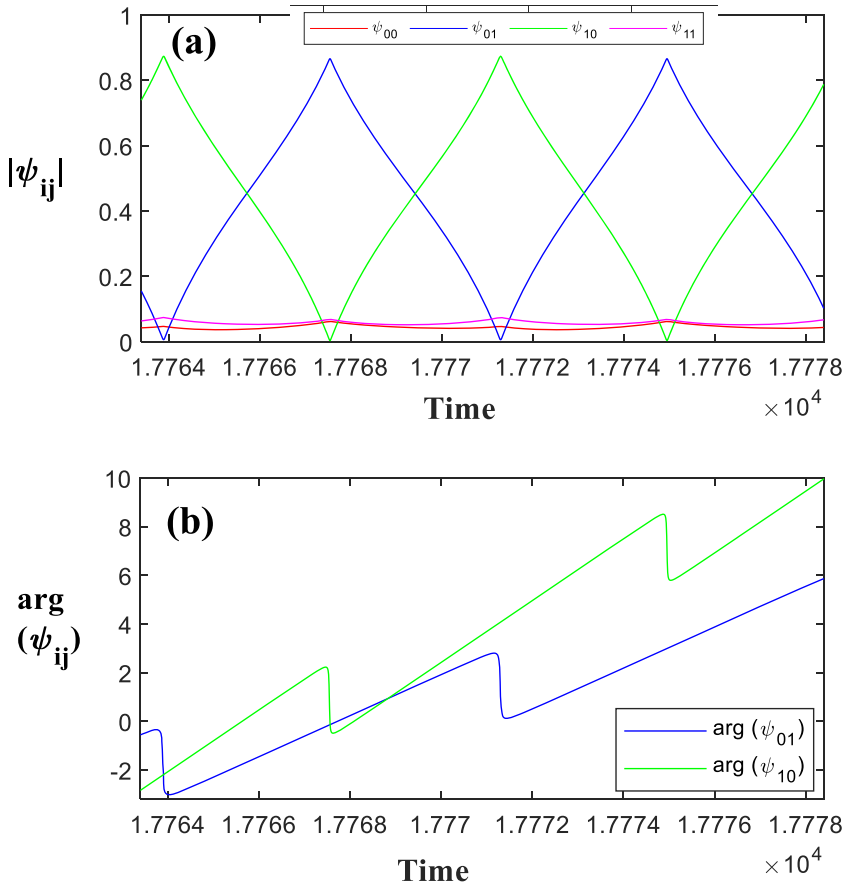

Figure 4. (a) Time dependence of the modulus of the complex coefficients, $\psi_{ij}, i, j = 0, 1$, and (b) time evolution of the phase of the coefficients ψ_{01} and ψ_{10}.

Equation (6) shows a rather interesting feature. For the case of a linear elastic system, it is obvious that the resultant elastic mode frequency is the same as the parent mode (i.e., the driving frequency). For such a system, n will be equal to 1 in equation (6) since no modal mixing is possible in a linear system. Hence, the complex coefficients will be independent of time. On the other hand, for the case of a nonlinear system, as is studied here, the complex coefficients are time-dependent since nonlinear mode-mixing is possible.

Figure 4(a) shows the time dependence of the complex coefficients, $\psi_{ij}, i, j = 0, 1$ at steady state. The components of ψ_{01} and ψ_{10} interact and exchange as time progress, however, the components of ψ_{00} and ψ_{11} are very small. Moreover, since both the complex coefficients ψ_{00} and ψ_{11} are small, whenever ψ_{01} and ψ_{10} are equal, we expect at that instant the state is maximally entangled (i.e., non-separable). On the other hand, if either ψ_{01} or ψ_{10} are close to zero, it is a separable state. From the phase values of ψ_{01} and ψ_{10} in figure 4(b), we observe a clear π jump in the geometric phase whenever the state becomes separable state. This evolution repeats periodically in time. Therefore, time enables the system to span its Hilbert space parametrically. The path the state vector $|\psi\rangle$ follows in $H_{E^{\mathrm{Al}},E^{\mathrm{Ac}}}$ is closed and periodic. The time evolution of the state vector which represents the accumulation of geometric phase can be reframed as the parallel transport of a vector [37] on a manifold constituted of a closed looped ribbon with

a single twist, that is, a Moebius strip. The sharpness of the π jump in time indicates that the twist is well localized along the strip.

3. Application to a phase-based mass sensor

We now investigate the influence of a mass defect on the time-dependent complex amplitudes of the granular network. For this, we emphasize the region where the phase of the complex amplitudes exhibits π jumps. We perturb the mass of the two granules forming the dumbbell on the right side of the network. Each granule is assigned a defected mass: $m_{\text{defect}} = m\left(1 - 7 \times 10^{-10}\right)$. We repeat the numerical experiment conducted in section 2 by calculating the time-dependent phases of the complex amplitudes while leaving all other system parameters the same.

We focus on the single time dependent complex component ψ_{01}, since it best captures the topology of the dynamics of the connected granular network. The phase of ψ_{01} (i.e., $\arg(\psi_{01})$) with and without mass defect is shown in figure 5(a). The mass defect is attempting to flatten the π jump. Effectively, it modifies the path the state vector $|\psi\rangle$ follows parametrically in the granular network's Hilbert space. This new path can be visualized as the parallel transport of a vector along a Moebius strip which twist extends over a longer segment of the strip. The twist associated with the defected system is more delocalized along the strip compared to that of the undefected system. To visualize this effect more clearly, we proceed to calculate the phase difference $\Delta(\arg(\psi_{01})) = \arg(\psi_{01})_{\text{with defect}} - \arg(\psi_{01})_{\text{without defect}}$. $\Delta(\arg(\psi_{01}))$ plot of figure 5(b) shows odd function character that follows a continuous cotangent graph with period π/ω_{D} and has a finite amplitude. We will show next that the width of $\Delta(\arg(\psi_{01}))$ versus time comes from the damping of the system, while the presence of the mass defect causes the magnitude of the cotangent like graph to be finite. Since the integral of a cotangent function is the natural log of a sine function, hence cumulative time-integral of the function $\Delta(\arg(\psi_{01}))$ (using cumulative trapezoidal rule as is shown in figure 5(c)) shows behavior similar to the natural log of a sine function. The influence of the mass defect causes a substantial fluctuation in the phases (in radians) as seen in figure 5(c).

In the next case, we double the system's damping parameter to better understand the effect of the system characteristics on the phases of the complex amplitudes with mass defect. Because the granular network under consideration is a highly nonlinear system, we must first identify the driving frequency value for which we may observe nonlinear eigen modes numerically, as shown in figure 2. This NNM frequency is found to be $\omega_{\text{D}} = 0.3667$.

We now consider the influence of the larger damping coefficient $\eta = \frac{4}{900}$ on the π jump before introducing mass-defect at the driving frequency $\omega_{\text{D}} = 0.3667$. In figure 6(a), we examine the time dependence of the phase of the complex amplitude ψ_{01} (i.e., $\arg(\psi_{01})$) with the two distinct driving frequency-damping coefficient combinations: $(\omega_{\text{D}}, \eta) = \left(0.4241, \frac{2}{900}\right)$ and $\left(0.3667, \frac{4}{900}\right)$. However, as previously stated, we obtain identical NNMs for both of these combinations of parameters (as shown in figure 2). Because the periods for these driving frequencies differ, we normalize time with respect to the relevant period in figure 6(a) to better contrast the results. Increasing damping reduces the sharpness of the π jump in figure 6(a). As a result, we can anticipate that higher damping systems will be less sensitive to mass changes than lower damping systems.

We now add a mass defect on the second dumbbell and calculate again the time dependency of the phase of the complex amplitude ψ_{01} ($\arg(\psi_{01})$), phase difference $\Delta(\arg(\psi_{01}))$, and cumulative time-integral of the function $\Delta(\arg(\psi_{01}))$ and compare the results with the

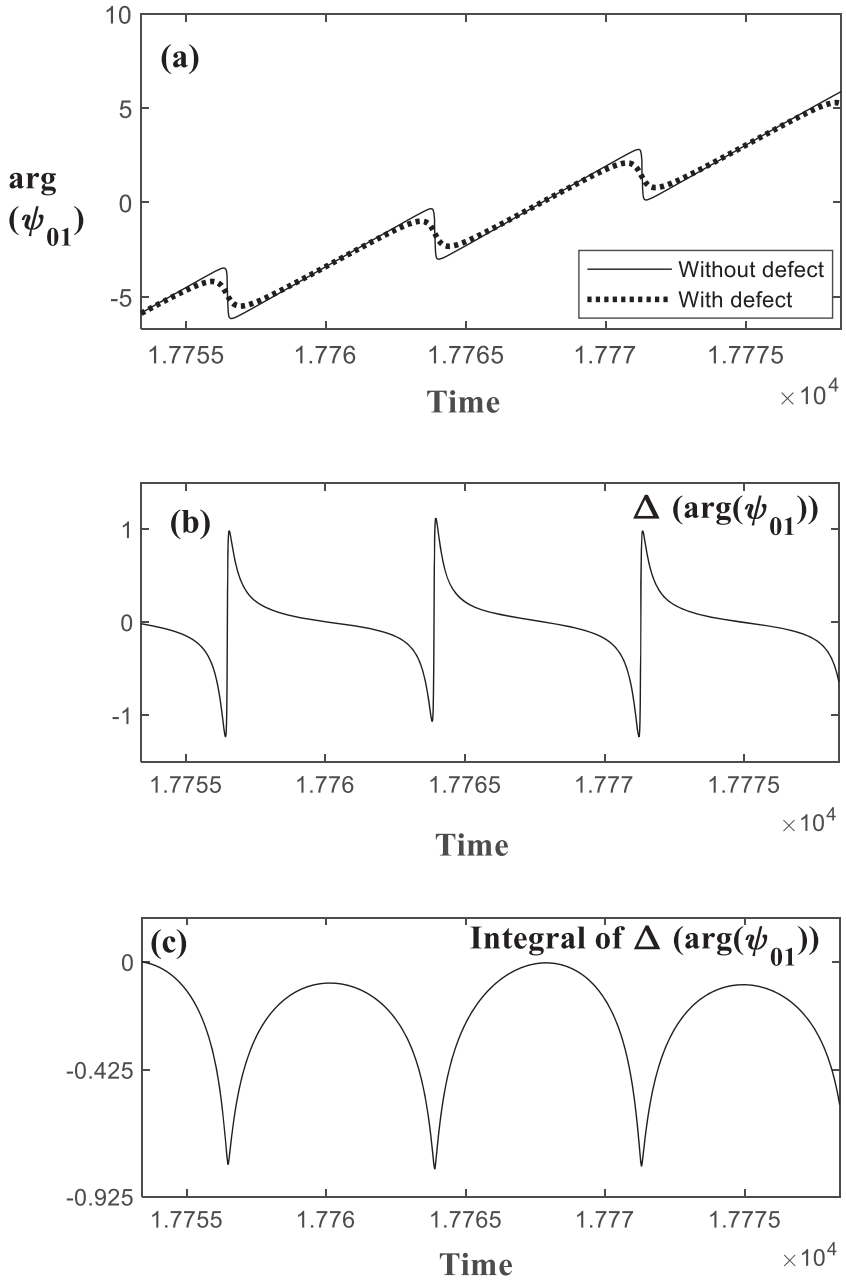

Figure 5. Time dependence of (a) the phase of the complex amplitude ψ_{01} i.e., $\arg(\psi_{01})$ with and without mass defect, (b) the phase difference $\Delta(\arg(\psi_{01})) = \arg(\psi_{01})_{\text{with defect}} - \arg(\psi_{01})_{\text{without defect}}$, and (c) cumulative time-integral of the function $\Delta(\arg(\psi_{01}))$.

system without the mass defect. Figure 6(b) depicts the cumulative time-integral of the function $\Delta(\arg(\psi_{01}))$ for various mass defect levels. The figure clearly indicates that bigger mass defects result in higher phase variations. However, comparing figures 5 and 6(b), we can

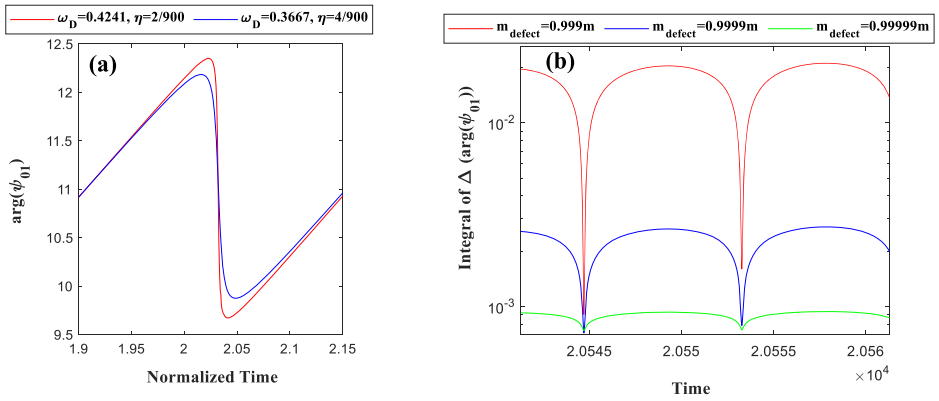

Figure 6. (a) Normalized time dependence of the $\arg(\psi_{01})$ for two distinct driving frequency and damping value combinations: $(\omega_D, \eta) = \left(0.4241, \frac{2}{900}\right)$ and $\left(0.3667, \frac{4}{900}\right)$ without the presence of a mass-defect, and (b) time dependence of the cumulative time-integral of the function $\Delta(\arg(\psi_{01}))$ for different values of the mass defect for $(\omega_D, \eta) = \left(0.3667, \frac{4}{900}\right)$, and with system parameters: $A_1 = \frac{1}{30}, \delta_0 = 0, A_2 = -A_1$.

see that a lower damping value has a higher sensitivity, that is, it can detect much smaller changes in mass.

4. Conclusions

We have conducted a modeling and dynamical simulation investigation of a nonlinear granular metamaterial composed of two pairs of granular dumbbells interacting linearly within the dumbbells and nonlinearly between dumbbells. When driven externally at some specific frequency, magnitude and distribution of applied forces, the nonlinear vibrational normal mode can be expressed in a linear normal mode orthonormal basis with time dependent complex coefficients. These coefficients constitute the components of a state vector in the 2^2 dimensional Hilbert space of the metamaterial and time enables the system to explore parametrically this Hilbert space along closed periodic paths. Along these paths, the components exhibit π jumps in the geometric phase that can be visualized as twists in the topological manifolds spanned parametrically by time. We demonstrated that these topological features can be exploited to realize mass sensor with very high sensitivity. The π jumps are extremely sensitive to the presence of mass defects. Mass flaws reduce the sharpness of the jumps as a function of time leading to measurable changes in geometric phase. The width of the jumps increases as the size of defects increases. As a result, there is no theoretical limit to the size of a defect that can be detected but the ability to measure small variations in phase. Dissipation may reduce the sensitivity of this metamaterial mass sensor. However, for metamaterials with very low damping one expects that extremely slight changes in mass may cause considerable sensitivity through large changes in geometric phase.

Acknowledgments

MAH thanks Wayne State University Startup funds for support. PAD was partially supported by National Science Foundation Emerging Frontiers in Research and Innovation (EFRI) Award (No. 1640860).

Data availability statement

The data generated and/or analysed during the current study are not publicly available for legal/ethical reasons but are available from the corresponding author on reasonable request.

Author contributions

All authors contributed equally to the research and writing of the manuscript.

Conflict of interest

The authors declare no competing interests.

ORCID iDs

M Arif Hasan https://orcid.org/0000-0001-7452-004X
Pierre A Deymier https://orcid.org/0000-0002-1088-7958

References

[1] Twiefel J, Glukhovkoy A, de Wall S, Wurz M C, Sehlmeyer M, Hitzemann M and Zimmermann S 2021 Towards a highly sensitive piezoelectric nano-mass detection—a model-based concept study *Sensors* **21** 7
[2] Lucklum R, Mukhin N, Djafari Rouhani B and Pennec Y 2021 Phononic crystal sensors: a new class of resonant sensors—chances and challenges for the determination of liquid properties *Front. Mech. Eng.* **7** 63
[3] Yang J J, Huang M, Tang H, Zeng J and Dong L 2013 Metamaterial sensors *Int. J. Antennas Propag.* **2013** e637270
[4] Hodaei H, Hassan A U, Wittek S, Garcia-Gracia H, El-Ganainy R, Christodoulides D N and Khajavikhan M 2017 Enhanced sensitivity at higher-order exceptional points *Nature* **548** 7666
[5] Fleury R, Sounas D and Alù A 2015 An invisible acoustic sensor based on parity-time symmetry *Nat. Commun.* **6** 5905
[6] Rosa M I N, Mazzotti M and Ruzzene M 2021 Exceptional points and enhanced sensitivity in PT-symmetric continuous elastic media *J. Mech. Phys. Solids* **149** 104325
[7] Berry M V 1984 Quantal phase factors accompanying adiabatic changes *Proc. R. Soc.* A **392** 45
[8] Lata T D, Deymier P A, Runge K, Le Tourneau F-M, Ferrière R and Huettmann F 2020 Topological acoustic sensing of spatial patterns of trees in a model forest landscape *Ecol. Model.* **419** 108964
[9] Hasan M A, Starosvetsky Y, Vakakis A F and Manevitch L I 2013 Nonlinear targeted energy transfer and macroscopic analog of the quantum Landau–Zener effect in coupled granular chains *Physica* D **252** 46
[10] Starosvetsky Y, Hasan M A, Vakakis A F and Manevitch L I 2012 Strongly nonlinear beat phenomena and energy exchanges in weakly coupled granular chains on elastic foundations *SIAM J. Appl. Math.* **72** 337
[11] Starosvetsky Y, Hasan M A and Vakakis A F 2013 Nonlinear pulse equipartition in weakly coupled ordered granular chains with no precompression *J. Comput. Nonlinear Dyn.* **8** 034504
[12] Hasan M A, Cho S, Remick K, Vakakis A F, McFarland D M and Kriven W M 2013 Primary pulse transmission in coupled steel granular chains embedded in PDMS matrix: experiment and modeling *Int. J. Solids Struct.* **50** 3207
[13] Lydon J, Jayaprakash K R, Ngo D, Starosvetsky Y, Vakakis A F and Daraio C 2013 Frequency bands of strongly nonlinear homogeneous granular systems *Phys. Rev.* E **88** 012206

[14] Hasan M A, Cho S, Remick K, Vakakis A F, McFarland D M and Kriven W M 2015 Experimental study of nonlinear acoustic bands and propagating breathers in ordered granular media embedded in matrix *Granul. Matter* **17** 49
[15] Nesterenko V F 2001 *Dynamics of Heterogeneous Materials* (New York: Springer)
[16] Nesterenko V F 1983 Propagation of nonlinear compression pulses in granular media *J. Appl. Mech. Tech. Phys.* **24** 733
[17] Starosvetsky Y, Jayaprakash K R, Hasan M A and Vakakis A F 2017 *Topics on the Nonlinear Dynamics and Acoustics of Ordered Granular Media* (Singapore: World Scientific)
[18] Starosvetsky Y and Vakakis A F 2010 Traveling waves and localized modes in one-dimensional homogeneous granular chains with no precompression *Phys. Rev.* E **82** 026603
[19] Jayaprakash K R, Starosvetsky Y, Vakakis A F, Peeters M and Kerschen G 2011 Nonlinear normal modes and band zones in granular chains with no pre-compression *Nonlinear Dyn.* **63** 359
[20] Starosvetsky Y, Jayaprakash K R, Vakakis A F, Kerschen G and Manevitch L I 2012 Effective particles and classification of the dynamics of homogeneous granular chains with no precompression *Phys. Rev.* E **85** 036606
[21] Maznev A A and Every A G 2011 Existence of backward propagating acoustic waves in supported layers *Wave Motion* **48** 401
[22] Kuznetsov S V 2019 Abnormal dispersion of lamb waves in stratified media *Z. Angew. Math. Phys.* **70** 175
[23] Kuznetsov S V 2022 Anomalous dispersion of lamb waves in Ge cubic crystal *Waves Random Complex Media* 1
[24] Bollinger J J, Itano W M, Wineland D J and Heinzen D J 1996 Optimal frequency measurements with maximally correlated states *Phys. Rev.* A **54** R4649
[25] Giovannetti V, Lloyd S and Maccone L 2004 Quantum-enhanced measurements: beating the standard quantum limit *Science* **306** 1330
[26] Giovannetti V, Lloyd S and Maccone L 2006 Quantum metrology *Phys. Rev. Lett.* **96** 010401
[27] Giovannetti V, Lloyd S and Maccone L 2011 Advances in quantum metrology *Nat. Photon.* **5** 4
[28] Lacarbonara W, Rega G and Nayfeh A H 2003 Resonant non-linear normal modes: I. Analytical treatment for structural one-dimensional systems *Int. J. Non-Linear Mech.* **38** 851
[29] Lacarbonara W and Rega G 2003 Resonant non-linear normal modes: II. Activation/orthogonality conditions for shallow structural systems *Int. J. Non-Linear Mech.* **38** 873
[30] Kerschen G, Peeters M, Golinval J C and Vakakis A F 2009 Nonlinear normal modes: I. A useful framework for the structural dynamicist *Mech. Syst. Signal Process.* **23** 170
[31] Ghose P and Mukherjee A 2014 Entanglement in classical optics *Rev. Theor. Sci.* **2** 274
[32] Hasan M A, Calderin L, Lata T, Lucas P, Runge K and Deymier P A 2019 The sound of bell states *Commun. Phys.* **2** 106
[33] Hasan M A, Runge K and Deymier P A 2021 Experimental classical entanglement in a 16 acoustic qubit-analogue *Sci. Rep.* **11** 24248
[34] Hasan M A, Calderin L, Lata T, Lucas P, Runge K and Deymier P A 2020 Experimental demonstration of elastic analogues of nonseparable qutrits *Appl. Phys. Lett.* **116** 164104
[35] Töppel F *et al* 2015 Classical entanglement: theory and application *2015 European Conf. on Lasers and Electro-Optics—European Quantum Electronics Conf.* (Optical Society of America) p EI_3a_3
[36] Hasan M A, Lata T, Lucas P, Runge K and Deymier P A 2022 Navigating the Hilbert space of elastic bell states in driven coupled waveguides *Wave Motion* **113** 102966
[37] Hobson M P, Efstathiou G P and Lasenby A N 2006 General relativity, an introduction for physicists https://cambridge.org/us/academic/subjects/physics/astrophysics/general-relativity-introduction-physicists, https://cambridge.org/us/academic/subjects/physics/astrophysics